



Cite this: *React. Chem. Eng.*, 2023, 8, 416

## Design and simulation of a uniform irradiance photochemical platform†

Dylan J. Walsh,  Timo N. Schneider,   
 Bradley D. Olsen  and Klavs F. Jensen \*

Received 16th August 2022,  
 Accepted 6th November 2022

DOI: 10.1039/d2re00329e

[rsc.li/reaction-engineering](https://rsc.li/reaction-engineering)

The growth of photochemistry and high throughput experimentation in well plates and flow drives interest in photochemical platforms that provide spatially uniform irradiation of reactions. Here, we present a design of a versatile, uniform light platform for photochemistry to enable increased performance and reproducibility for high throughput experimentation in shallow well plates, in-plane flow reactors, and droplets. The design of the platform is driven by the development of an open-source ray tracing light simulation package. Radiometry provides experimental validation of the system's irradiance and irradiance uniformity. The usefulness of the approach is demonstrated by application to the photoinduced electron transfer–reversible addition–fragmentation chain transfer polymerization of methyl acrylate.

## Introduction

The increasing access to low-cost LEDs has rekindled interest in photochemistry with a particular focus on the development of new catalytic systems that perform well under visible light.<sup>1–4</sup> These systems enable new chemical transformations under mild conditions, which have made them useful in many applications from pharmaceutical synthesis<sup>1,4,5</sup> to 3D printing<sup>6–9</sup> to disease diagnostics through signal amplification.<sup>10–12</sup> However, variations in performance of these systems with the configuration of experimental setups have created challenges.<sup>5,13–15</sup> The number of photons absorbed by the reaction mixture depends on several factors including light intensity, emission profile of the light source, distance from the light source, geometry of the light, vessel, and surrounding environment and how fast the reaction is mixed.<sup>13,16–22</sup> This complexity challenges the transferability of reaction conditions and reproducibility of photochemistry experiments. The issue becomes even more important in high throughput experimentation in which well plates, multiple vials, and flow reactors are used to run large numbers of reactions at high photon flux.<sup>5,13,23</sup>

In order to address these issues, several custom photochemical platforms tailored for high throughput experimentation have been reported by commercial vendors as well as research labs.<sup>13,15,16,19,21,22,24–34</sup> A large fraction of these platforms are designed for vials and seek to maximize

photon flux by placing LEDs as close as possible to vials and/or coating all surfaces with reflective material.<sup>13,27,29</sup>

Common approaches for flow reactors have focused on matching LED position to flow paths, wrapping the reactor around a light source, or placing the light source around the reactor.<sup>16,26,35</sup> Photochemical platforms for well plates most commonly place a single LED above/below every well or use light diffusers above a small number of lights.<sup>30</sup> A few recent approaches have sought to provide more versatile platforms that can illuminate multiple different setups.<sup>24,25,28</sup> While there have been many photoreactors reported before and shown to perform well for specific photochemical transformations, these designs did not fully address our research needs at the time our project started.

Herein, we present and validate a versatile photochemical system for reactions done in well-plates or in-plane channels with uniform illumination from above. The design consists of high-powered LEDs arranged in an array surrounded by mirrors on all four sides (Fig. 1). The optimal configuration of the design is driven by open-source ray tracing Python programs we developed. The uniform irradiance of the platform is validated experimentally by radiometry. Finally, the new photochemical platform is applied to the photoinduced electron transfer–reversible addition–fragmentation chain transfer polymerization of methyl acrylate in well plates, continuous droplet flow, and droplet stop–flow.

## Results and discussion

### Design of photochemical platform

We set out to design a general photochemical platform to uniformly irradiate well plates, flow, and droplet stop–flow reactors (Fig. 1). For well plates, the platform needs to

Department of Chemical Engineering Massachusetts Institute of Technology, 77 Massachusetts Avenue, Cambridge, Massachusetts 02139, USA.

E-mail: [kfjensen@mit.edu](mailto:kfjensen@mit.edu)

† Electronic supplementary information (ESI) available. See DOI: <https://doi.org/10.1039/d2re00329e>



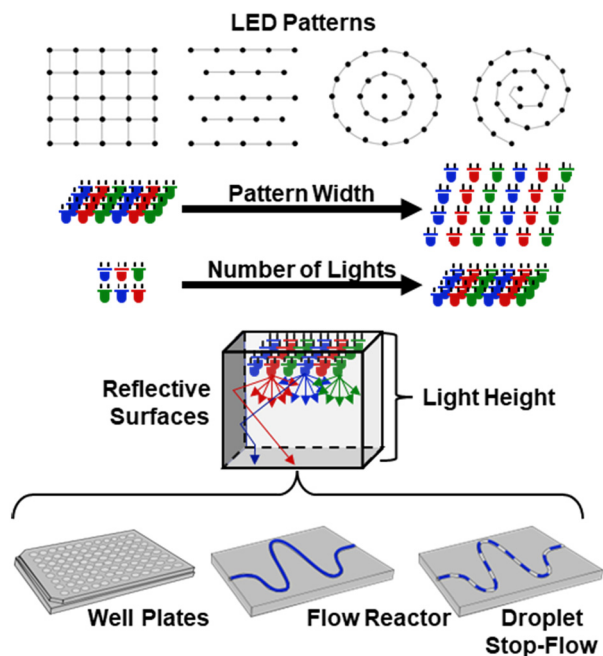


**Fig. 1** Overview of the design parameters of the photochemical system to be optimized. The design parameters include LED pattern, pattern width, number of LEDs, height of the LEDs, and the addition of reflective surfaces.

provide reproducible reactivity across all wells and handle any well plate design or well count. For flow reactors, the platform needs to be able to support the reconfiguration of the flow path for different reactor lengths or diameters in a plane. For stop-flow reactions, the droplets may be stopped anywhere within the reactor flow path and need to produce equivalent results in all locations. Additionally, the photochemical platform should be compatible with automated systems, such as a robot arm to exchange well plates, or be integrated into a larger (stop-)flow system. Given that the desired reactor configurations of the system can all be aligned on a single plane, a planar light source was proposed. Specifically, multiple LEDs arranged in a grid-like pattern would irradiate directly down to the well plate, flow reactor, or droplet system (Fig. 1). This design is simple and enables easy access for a robot arm and provides ample room for cooling solutions to minimize the effect of energy given off by the LEDs and absorbed in the reactors. To guide the design of the photochemical platform further, the following additional design criteria were set:

- **Highly uniform irradiance:** the platform is designed for well plates, flow chemistry, and stop-flow chemistry. Given the diversity of situations, the platform will be used for, uniform irradiance is needed to ensure reproducible reactions.
- **High irradiance intensity:** a high photon flux shortens reaction times, which enables high throughput experimentation. Additionally, some chemistries require a high level of irradiance for productive catalysis.

- **Tunable irradiance:** a high level of irradiance can be deleterious for some chemistries, thus the ability to control the level of irradiance offers flexibility in performing different chemistries.

- **Multiple wavelengths:** multiple wavelengths increase the platform's flexibility to run different chemistries and catalysts.

- **Computer control:** computer control enables the light setup to be integrated into larger automation platforms.

- **Safe:** high-power LEDs can generate a large amount of heat which requires the incorporation of cooling systems and engineering safety measures. Only visible light LEDs are used to avoid the dangers of UV light.

With a planar light source, there are several design parameters such as the number and spatial position of the LEDs that need to be determined to maximize irradiance and irradiance uniformity (Fig. 1). Additionally, understanding the effects of adding optical elements such as diffusers or mirrors on irradiance and irradiance uniformity will be important to achieve an optimal design.

We considered performing ray tracing analysis on possible configurations to gain insights into the optimal design of the photochemical platform. While there is commercial software available to perform this analysis, we aspired to support the growth of open-source software and created a ray tracing Python software package (see the ESI† for details).<sup>36</sup> The ray tracing algorithm works by casting rays of light from each light source and tracing their path through the 3-dimensional environment until they are absorbed by a surface. The ray tracing package has support for reflective surfaces, transmitting surfaces (with scattering), and non-uniform light sources. The code has several optimizations for performance and implements Numba to allow for 'just-in-time' compiling to accelerate computations.<sup>37</sup> With the optimizations in place the algorithm typically runs in about a minute. The ray tracing Python package was validated against the inverse square law, cosine law, and the irradiance profiles for a uniform point source and a non-uniform point source with mirrors on a flat surface with analytical solutions (see ray tracing code in ESI† for details).

The first photochemical platform parameter to determine for the planar light source design is the optimal *xy*-LED position. Prior literature focused on placing LEDs strategically above the flow path or directly centered on individual wells in a well plate, but this approach locks the setup to a single configuration, limiting the versatility.<sup>16,26,35</sup> Four generic LED light patterns were explored: concentric circles, spirals, a grid, and an offset grid (see ESI† grids for more details). However, to make a conclusion about the best LED pattern, the other parameters must also be simultaneously considered as there are dependent effects. The parameters that were explored were the number of lights [4, 16, 36, 49, 81], light height [10, 20, 30, 50, 100, 150] mm, and light pattern width [75, 100, 125, 150] mm with no additional optical elements (like mirrors). A total of 480 ray tracing simulations were performed. For each simulation, 5



million rays were traced through the simulation, and the mean and standard deviation (std) of rays absorbed on the 100 mm  $\times$  100 mm surface were calculated. The plot of the convex hull/envelope in std/mean space for each of the grid patterns (Fig. 2a) provides a visual representation of the space covered by each grid pattern. In the std/mean space, the lower bound of the convex hull is the area of the most interest as this bound represents the more uniform illumination for a given mean irradiance. All four patterns have similar lower bounds in low to mean irradiance range, and at the higher mean intensity range the grid and offset grid perform slightly better. Thus, the grid pattern does not make a significant difference, with the assumption that the other parameters are optimized.

Focusing on the offset grid, we investigated the effect of height of the lights off the surface, and a clear decrease in mean intensity is observed (Fig. 2c). This decrease in mean intensity falls in the transition regime between an area light source and a point light source (see ESI† Fig. S15). The std of irradiance decreases with increasing height due to each light irradiance being spread over an increasing area. However, looking at the std normalized to mean irradiance shows that a minimum occurs at 20 mm. This minimum can be explained by very intense hot spots when the lights are too close to the surface, whereas when the lights are far from the surface the intensity drops rapidly and outpaces the improvement in uniformity. Lastly, with an increasing width

of the light pattern both the mean and the std irradiance decrease. If we once again look at std normalized to the mean irradiance, the trend suggests that wider patterns result in more uniform irradiance, but this also has diminishing returns. To conclude these results, it is apparent that there is an ideal height to put the light source above the surface, increasing the number of lights is always beneficial, and increasing the width of the lighting pattern results in a tradeoff between irradiance intensity vs. uniformity.

To investigate the possible benefit of optical elements for the photochemical platform, we explored the use of light diffusing layers and reflective surfaces. For a light diffusing layer, we choose ground glass as it is common in many light setups and has data characterizing its optical behavior (see ESI† emission and transmittance profiles for more details).<sup>38,39</sup> To determine the effect of the diffuser, a 300 mm  $\times$  300 mm diffuser was placed in between the lights and a 100 mm  $\times$  100 mm absorbing surface. Ray tracing simulations were performed revealing that height of the diffuser layer only had a minor effect (<1% change) on mean and std with a placement closer to the lights preferable. To determine if the diffuser layer was beneficial, the convex hull of std/mean was calculated with and without the diffuser layer. Fig. 3 shows that the diffuser does not significantly change the lower bound of the convex hull. A deeper analysis of 2D heat maps shows that at a given light setup, adding the diffuser layer does indeed improve uniformity, but at a huge

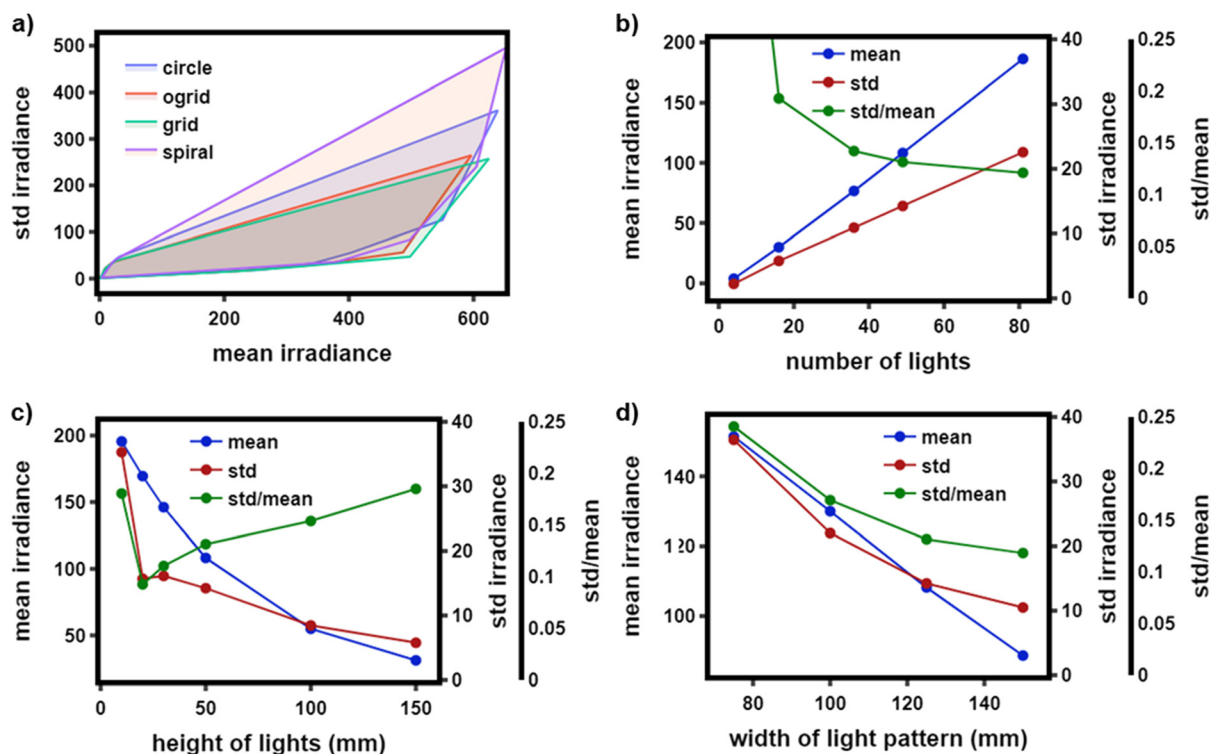


Fig. 2 a) Convex hull for each grid type in the std/mean irradiance space. b) Dependence of mean and std on number of lights for the offset grid light pattern at a light height of 50 mm and with a pattern width of 125 mm. c) Dependence of mean and std on height of lights for the offset grid light pattern with 46 lights and a pattern width of 125 mm. d) Dependence of mean and std on the width of the light pattern for the offset grid light pattern with 46 lights at a height of 50 mm (std: standard deviation).



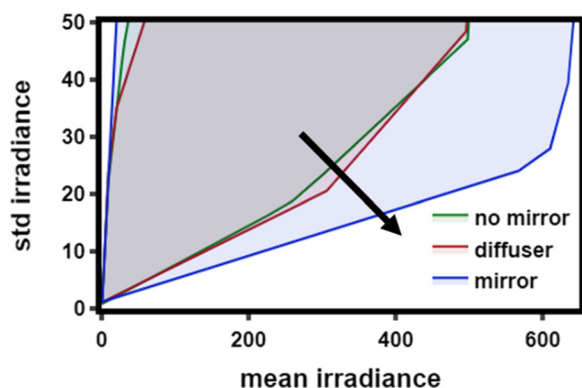


Fig. 3 Convex hull for the offset light grid with and without diffuser or mirrors in the std/mean irradiance space. The arrow indicates the region that is most beneficial (high uniformity and light intensity) for the convex hull to expand into.

cost to light intensity effectively resulting in no improvement.

To evaluate the effectiveness of reflective surfaces, we investigated mirrors placed on all 4 sides of the light setup. A mirror efficiency of 85% was used as that is typical for low-cost materials.<sup>40</sup> Results reveal that placing mirrors as close to the lights as possible maximizes the mean irradiance, and std irradiance is not significantly affected by changes in the mirror offset. The convex hull over the std/mean irradiance space for the mirrors was found to significantly decrease the lower bound of the convex hull (Fig. 3). This result shows that adding mirrors significantly improved the uniformity of the irradiance for a given mean irradiance. Looking at the simulation results more closely, the non-mirror heat maps (see ESI† Fig. S20) revealed that the corners and edges of the surfaces had lower irradiance than the center. Thus, the addition of the mirrors enables light that otherwise would have missed the surface to be reflected to illuminate these areas, as well as the center, but to a much lesser effect. With the addition of mirrors, there is a significant reduction in the effect of irradiance with respect to the height of the lights which provides flexibility in light placement in the photochemical platform design. Moreover, the reflected light redirected back to the surface is quite significant resulting in nearly a doubling of intensity in many of the cases studied. To evaluate the benefits of a higher quality mirror, a perfect 100% efficiency mirror box was simulated (see ESI† Fig. S21). The increase in reflecting efficiency resulted in a ~15% increase in mean irradiance at the optimal light height, with the irradiance uniformity not significantly affected. Overall, mirrors both increase mean irradiance and improve irradiance uniformity making them a must for experimental setups.

Combining the conclusions obtained from the ray tracing studies, we chose a specific design of 46 LEDs in an offset grid pattern with a width of 125 mm and mirrors on all four sides (Fig. 4). To get a high level of irradiance, LUMILEDS Luxeon C Color Line LEDs were used because

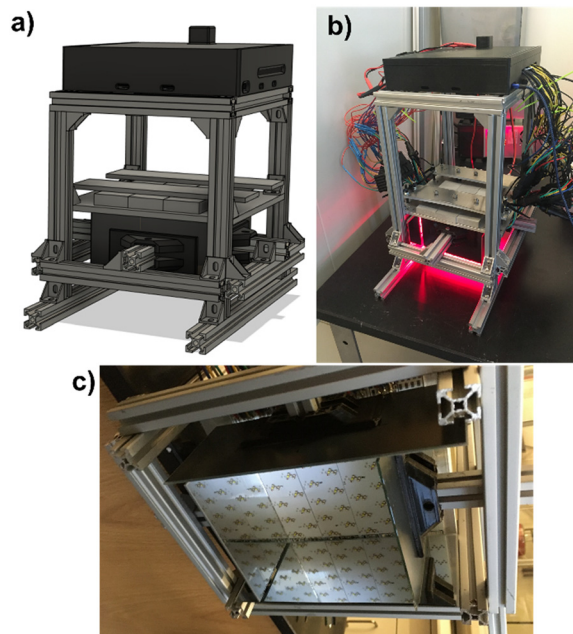


Fig. 4 a) Computer aid design renderings of the photochemical platform. b) Photograph of the assembled photochemical platform with red LEDs on. c) Photograph from the bottom of the photochemical platform to show the array and mirrors.

the small size (2 mm × 2 mm) allows for a high density of lights. They are high power and come in 13 color options ranging from violet to far red. We specifically chose 6 different color LEDs as this provides sufficient coverage of wavelengths from 420–670 nm (full visible spectrum). To support the 6 colors of LEDs in an offset grid pattern, a custom aluminum PCB (printed circuit board) was made with each grid position containing a cluster of the 6 colors. The aluminum PCB was chosen to help dissipate the significant amount of heat generated by the LEDs. The LED PCB is attached to an aluminum plate with thermal paste to further facilitate the dissipation of heat from the LEDs. Water blocks (water circulation system) were used on the back side of the aluminum plate to actively remove heat away from the LEDs. The PCB contains 3 additional connections for surface-mounted thermocouples to monitor the temperature. To drive the high-power LEDs, the PicoBuck LED driver from Sparkfun was used as it provides the ability to control the current delivered to the LEDs with the use of a PWM (pulse wave modulation) signal, thus satisfying the tunable irradiance design criteria. The LED drivers are capable of driving 7 LEDs in series at 36 V, up to 1 Amp. To provide DC power to the LED drivers 36 V (10 Amps) Mean Well DC power supplies were used. A Raspberry Pi Pico microcontroller was used to provide the PWM signals to for the LED driver, and the built-in analog-to-digital (ADC) converter is used to read the thermistors on the LED PCB. The Pico was chosen for its low-cost, support for Micropython, and the presence of a hardware watchdog. The Pico is programmed to shut off the LEDs in





the case of overheating as the first engineering fail-safe. The hardware watchdog is the second engineering control, which will automatically reset the microcontroller and LED array in the case of a software or hardware failure. All the electronics were packaged into a custom 3d printed box, and the whole LED assembly was mounted and supported with 2020 aluminum extrusion. The aluminum extrusion enables the height of the LEDs and the position of the mirrors to be quickly adjusted and easily swapped. Additionally, the aluminum extrusion construction supports the incorporation of the photochemistry platform into larger automated systems. The use of mirrors enables the chemical system to be placed further from the LEDs to reduce the effect of heat generated by the LEDs. Additionally, the setup has plenty of space for air to be blown up one side of the mirror box and out the other to further reduce the effects of heat generation of the LEDs. While we have chosen a specific design here, if a larger or smaller, higher power, *etc.* platform is needed, the system can be re-scaled, and ray tracing calculations can be rerun to determine the optimal design for that scale.

## Experimental validation

Radiometry was used to provide a quantitative analysis of the light irradiance and uniformity of the photochemical platform. To use a radio-spectrometer to evaluate the irradiance and uniformity, the lens of the radio-spectrometer was attached to a computer-controlled *x-y* stage to enable raster scanning (see ESI† radiometry for more details). The analysis was performed over a 180 mm × 180 mm square area with data points every 10 mm (324 points total) both with and without mirrors. A light height of 90 mm and mirrors of 80 mm in length were used so that the radio-spectrometer lens clears the bottom of the mirrors during rastering. For the experimental setup without mirrors, a smooth 2d Gaussian-like distribution with a maximum ( $5.5 \text{ W m}^{-2}$ ) in the middle was observed (Fig. 5a). Simulating irradiance for the same setup with the ray tracing algorithm produced a nearly identical result (Fig. 5b). For the setup with the mirrors, uniform irradiance is observed within the area within the mirrors (Fig. 5c), and simulations give nearly identical results to the experiment. Additionally, the

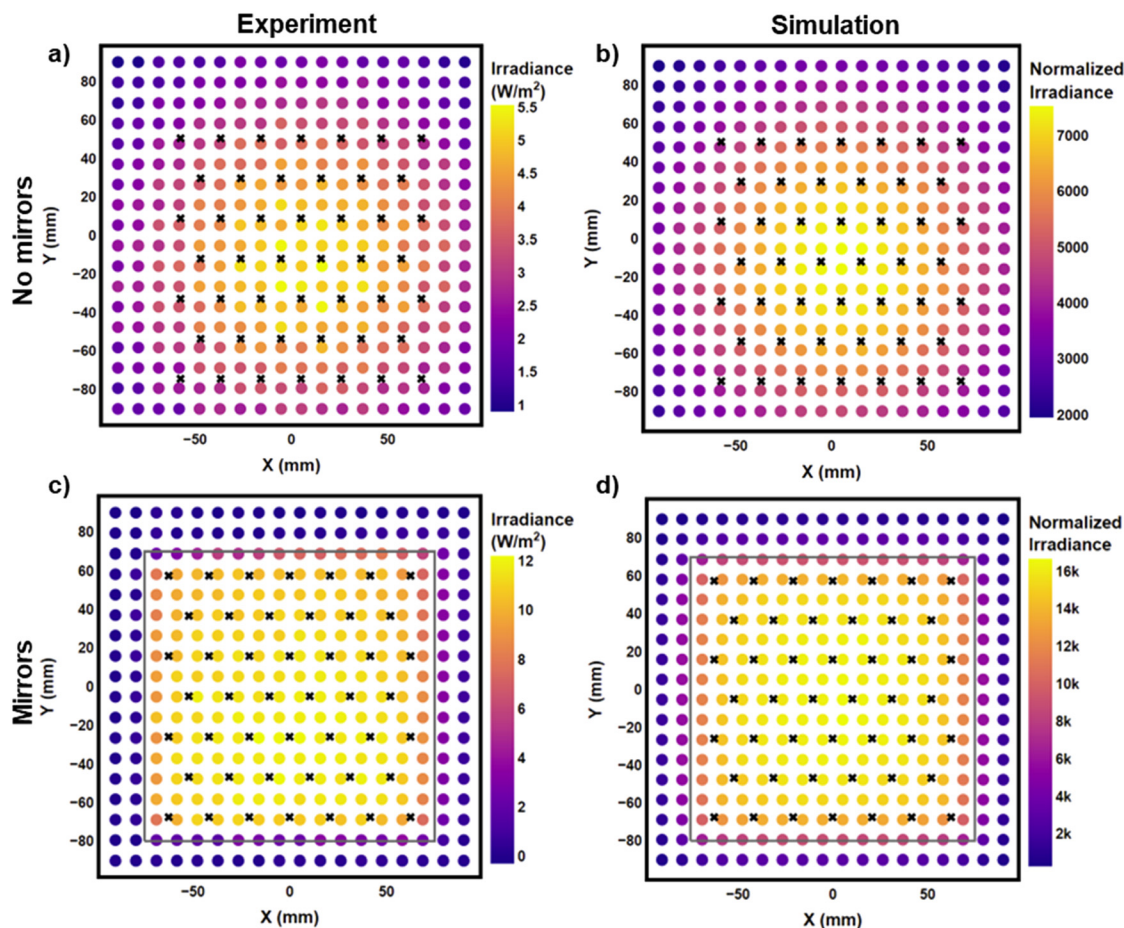


Fig. 5 Plots of the radiometry data for the experimental setup and simulation with and without mirrors. Red LEDs were used in the experiment at 1% power. a) Experimental results with no mirrors. b) Simulation results with no mirrors. c) Experimental results with mirrors. d) Simulation results with mirrors. The black 'x's signify the locations of LEDs. The gray 'box' signifies the location of the mirrors.



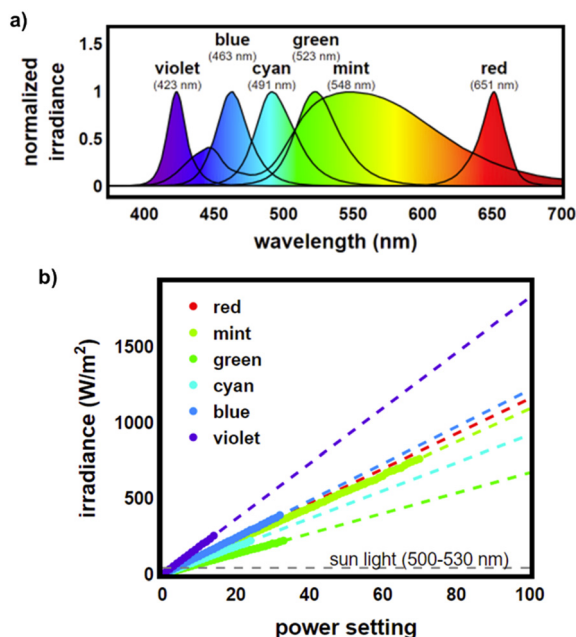


Fig. 6 a) Normalized emission spectra for each color LED on the photochemical platform. b) Irradiance vs. power setting for all 6 LED colors. Measurements were taken at 80 mm below the light setup with mirrors. Data points were taken starting at the lowest power setting and increasing until the detector reached its max irradiance limit. Linear fits were applied to the data collected and projected to the max power setting.

maximum irradiance increased from  $5.5 \text{ W m}^{-2}$  in the no-mirror situation to  $12 \text{ W m}^{-2}$  with the mirrors. This drastic improvement is in-line with the conclusion provided by the simulation. The maximum values between the mirrors and no mirrors situation for the experiment  $(12 \text{ W m}^{-2})/(5.5 \text{ W m}^{-2}) = 2.18$  and the simulation yields  $(16\,600/7500) = 2.21$  are in good agreement.

Radiometry was used to quantify the irradiance for each color of LED (Fig. 6). Measurements were taken starting at the lowest power setting and increasing until the signal grew larger than the radiometer max limit. Irradiance appeared to be linear with respect to the power setting, thus a line was fitted and projected to the max power setting (for more details see ESI† radiometry). The use of high-power LED in our platform yields maximum irradiances ranging from  $671 \text{ W m}^{-2}$  for green up to  $1830 \text{ W m}^{-2}$  for violet. This is considerably more powerful than an equivalent 30 nm swath of sunlight ( $42 \text{ W m}^{-2}$  for 500–530 nm), and significantly more powerful than many reported photochemical setups. Combining the radiometric results confirm that the design criteria for a high level of uniform irradiance at high power were successfully achieved.

### Application to photo-polymerization

The photoinduced electron transfer–reversible addition–fragmentation chain transfer (PET–RAFT) polymerization served to demonstrate the utility of the photochemical

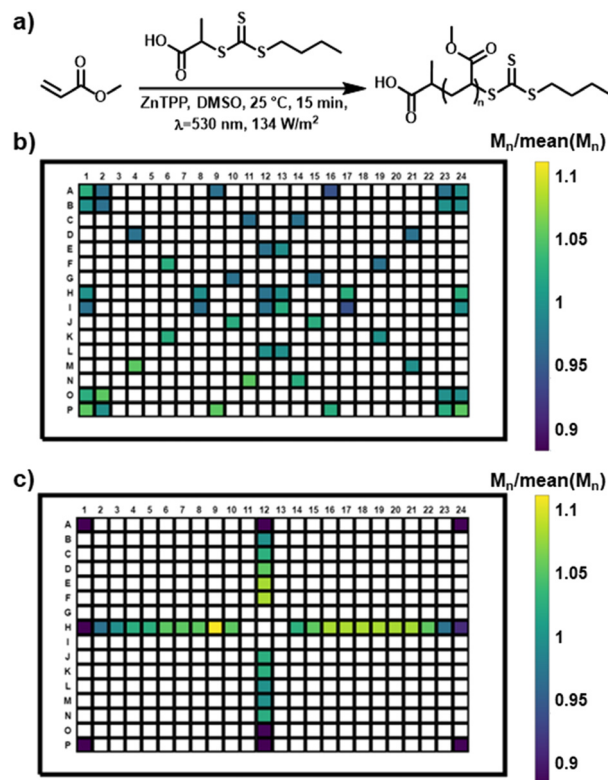


Fig. 7 a) Reaction scheme for the PET–RAFT polymerization of methyl acrylate. b) Diagram of the  $M_n/\text{mean}(M_n)$  results for the PET–RAFT polymerization in 384 well plate. c) Diagram of the  $M_n/\text{mean}(M_n)$  results for the PET–RAFT polymerization in 384 well plate with the mirrors removed from the photo-platform. The white color indicates empty wells.

platform (Fig. 7a).<sup>41</sup> Specifically, 52 identical polymerizations of methyl acrylate in the presence of zinc tetraphenylporphine (ZnTPP) and 2-(((butylthio)carbonothioyl)thio)propanoic acid (BTPA) dissolved in DMSO (see ESI† polymerizations for more details) were performed. The reactions were patterned across a 384 well plate to test the reproducibility of reactions. The well plate was set 80 mm below the lights and irradiated with green light (523 nm,  $134 \text{ W m}^{-2}$ , 20% setting) for 10 minutes. The polymerizations were analyzed by size exclusion chromatography (SEC) yielding an average  $M_n$  of  $11\,000 \text{ g mol}^{-1}$  with a dispersity of 1.10. Taking a closer look at the polymer's molecular weight as a function of the polymerization's position (Fig. 7b) shows no significant variation. The standard deviation of  $M_n$  across all reactions was  $253 \text{ g mol}^{-1}$  or 2.3%. The polymerizations were exposed for an additional 5 minutes, and a sample was taken producing an  $M_n$  of  $12\,700 \text{ g mol}^{-1}$  with a dispersity of 1.11 which matches literature values ( $M_n$ :  $12\,700 \text{ g mol}^{-1}$  and a dispersity of 1.09 at full conversion).<sup>41</sup> A second set of identical polymerizations was setup and irradiated for 15 min. The second set of polymerizations yielded an average polymer  $M_n$   $12\,800 \text{ g mol}^{-1}$  with a dispersity of 1.11, showing the good reproducibility of the platform between plate runs. Note that the literature example took 2 hours under a 5 W



light in vials, whereas the reaction was done in 15 min in the new system showcasing the benefit of higher light intensity. With high-intensity light, the concentration of radicals increases which can lead to side and termination reactions.<sup>42</sup> To demonstrate the retention of trithiocarbonate end-groups, the chain extension of poly(methyl acrylates) (PMA) was carried out to yield homo-diblock copolymers (PMA-*b*-PMA). SEC revealed a complete shift of the starting block to lower retention time with low dispersity ( $<1.12$ ) (see ESI† Fig. S36) supporting the high fidelity of the end-group at high light intensity. The high reproducibility of the polymerization across the well plate and the high quality of the material produced support the uniform radiometry results and the utility of the experimental setup.

To explore the effects of heterogeneous illumination, the mirrors of the photochemical platform were removed to create a 2d Gaussian-like distribution of irradiance. In a 384 well plate, 38 identical PET-RAFT polymerizations were performed by irradiating the reactions with green light (523 nm,  $134 \text{ W m}^{-2}$ , 20% setting) for 10 minutes. The polymerizations were analyzed by size exclusion chromatography (SEC) yielding an average  $M_n$  of  $5740 \text{ g mol}^{-1}$  with a dispersity of 1.09. The significantly lower  $M_n$  is consistent with radiometry and simulation results, which suggested a  $\sim 2.2$  drop in irradiance with the removal of the mirrors. Taking a closer look at the polymer's molecular weight as a function of the polymerization's position in the well plate (Fig. 7c) shows a decrease in  $M_n$  that corresponds with the decreasing light intensity, which is to be expected from the kinetics of PET-RAFT.<sup>42</sup> The dispersity remained narrow ( $>1.1$ ) for all wells, which can be rationalized by the fact that irradiance does not vary significantly across a single well and the wells are small enough for diffusion to minimize any minor heterogeneities that arise.

To illustrate the versatility of the platform, the PET-RAFT polymerization was performed in droplet continuous-flow and droplet stop-flow (Fig. 1 and S37†). A flow reactor was constructed from PFA (perfluoroalkoxy alkane) tubing and two syringe pumps. One syringe pump was used to feed air or  $\text{N}_2$ , while the second syringe pump was used to flow the same PET-RAFT polymerization reaction mixture used for the well plate experiments, except at a higher dilution of 1 M (based on monomer) to avoid viscosity issues.<sup>43–45</sup> The continuous-flow experiments were performed by feeding the reaction mixture and gas at  $50 \mu\text{L min}^{-1}$  (10 min residence time) into the reactor being irradiated with green light (523 nm,  $134 \text{ W m}^{-2}$ , 20% setting). At steady state, samples were collected and analyzed every 2 minutes for a 10 minute period. Analysis of the 5 samples yielded an  $M_n$  of  $8180 \text{ g mol}^{-1}$  with a standard deviation of  $60 \text{ g mol}^{-1}$  and a narrow dispersity of 1.07 supporting the high reproducibility of the platform for flow. An additional experiment was conducted where the light intensity was varied between 13.2 and  $670 \text{ W m}^{-2}$  to demonstrate how the platform can be used for kinetic experiments (see ESI† Fig. S38). The droplet stop-flow experiment was performed by creating droplets using the

continuous-flow droplet conditions and stopped when a steady state was reached. The stopped droplets were then exposed for 10 minutes to green light (523 nm,  $134 \text{ W m}^{-2}$ , 20% setting) and 10 samples were collected. Analysis of the samples yielded an  $M_n$  of  $7930 \text{ g mol}^{-1}$  with a standard deviation of  $160 \text{ g mol}^{-1}$  and a dispersity of 1.07. The low standard deviation of molecular weight provides additional support for uniform irradiance as each droplet was stopped in a different location in the photochemistry platform, and thus could have experienced different amounts of light intensity if the light intensity varied. These results demonstrate the photochemistry platform's ability to switch between various experimental setups and provide uniform levels of irradiance.

## Conclusions

We have presented the design of a versatile uniform photochemistry platform. The use of a custom open-source ray tracing software was used to determine the optimal design of the platform. Among the key findings was the benefit of mirrors for both increasing the light irradiance as well as significantly increasing light uniformity. This conclusion held up well when it was experimentally validated with radiometry. Finally, we demonstrated the utility of the platform for photo-polymerizations. We are making the techniques and designs available for other experimentalist to implement photochemistry platforms.

## Author contributions

Walsh: conceptualization, data curation, formal analysis, investigation, methodology, software, validation, visualization, writing – original draft, writing – review & editing. Schneider: formal analysis, validation, writing – review & editing. Olsen: funding acquisition, project administration, supervision, validation, writing – review & editing. Jensen: funding acquisition, project administration, supervision, validation, writing – review & editing.

## Conflicts of interest

There are no conflicts to declare.

## Acknowledgements

This work was funded by the NSF Convergence Accelerator award number 2134795.

## Notes and references

- 1 Y. Su, N. J. W. Straathof, V. Hessel and T. Noël, *Chem. – Eur. J.*, 2014, **20**, 10562–10589.
- 2 N. Corrigan, S. Shanmugam, J. Xu and C. Boyer, *Chem. Soc. Rev.*, 2016, **45**, 6165–6212.
- 3 C. Wu, N. Corrigan, C.-H. Lim, W. Liu, G. Miyake and C. Boyer, *Chem. Rev.*, 2022, **122**, 5476–5518.





- 4 A. Y. Chan, I. B. Perry, N. B. Bissonnette, B. F. Buksh, G. A. Edwards, L. I. Frye, O. L. Garry, M. N. Lavagnino, B. X. Li, Y. Liang, E. Mao, A. Millet, J. V. Oakley, N. L. Reed, H. A. Sakai, C. P. Seath and D. W. C. MacMillan, *Chem. Rev.*, 2022, **122**, 1485–1542.
- 5 D. Cambi , C. Bottecchia, N. J. W. Straathof, V. Hessel and T. No l, *Chem. Rev.*, 2016, **116**, 10276–10341.
- 6 J. R. Tumbleston, D. Shirvanyants, N. Ermoshkin, R. Januszewicz, A. R. Johnson, D. Kelly, K. Chen, R. Pinschmidt, J. P. Rolland, A. Ermoshkin, E. T. Samulski and J. M. DeSimone, *Science*, 2015, **347**, 1349–1352.
- 7 L. Zhou, J. Fu and Y. He, *Adv. Funct. Mater.*, 2020, **30**, 2000187.
- 8 M. Layani, X. Wang and S. Magdassi, *Adv. Mater.*, 2018, **30**, 1706344.
- 9 A. Bagheri and J. Jin, *ACS Appl. Polym. Mater.*, 2019, **1**, 593–611.
- 10 K. Kaastrup and H. D. Sikes, *Chem. Soc. Rev.*, 2016, **45**, 532–545.
- 11 S. Kim, A. M. Dibildox, A. Aguirre-Soto and H. D. Sikes, *J. Am. Chem. Soc.*, 2021, **143**, 11544–11553.
- 12 S. Kim and H. D. Sikes, *Polym. Chem.*, 2020, **11**, 1424–1444.
- 13 C. “Chip” Le, M. K. Wismer, Z.-C. Shi, R. Zhang, D. V. Conway, G. Li, P. Vachal, I. W. Davies and D. W. C. MacMillan, *ACS Cent. Sci.*, 2017, **3**, 647–653.
- 14 L. Buglioni, F. Raymenants, A. Slattey, S. D. A. Zondag and T. No l, *Chem. Rev.*, 2022, **122**, 2752–2906.
- 15 C. P. Haas, T. Roeder, R. W. Hoffmann and U. Tallarek, *React. Chem. Eng.*, 2019, **4**, 1912–1916.
- 16 A. Roibu, R. B. Morthala, M. E. Leblebici, D. Koziej, T. van Gerven and S. Kuhn, *React. Chem. Eng.*, 2018, **3**, 849–865.
- 17 M. Sender, B. Wriedt and D. Ziegenbalg, *React. Chem. Eng.*, 2021, **6**, 1601–1613.
- 18 M. Sender and D. Ziegenbalg, *React. Chem. Eng.*, 2021, **6**, 1614–1627.
- 19 D. Cambi , F. Zhao, V. Hessel, M. G. Debije and T. No l, *React. Chem. Eng.*, 2017, **2**, 561–566.
- 20 D. Ziegenbalg, A. Pannwitz, S. Rau, B. Dietzek-Ivan    and C. Streb, *Angew. Chem.*, 2022, **61**, e202114106.
- 21 D. Kowalczyk, P. Li, A. Abbas, J. Eichhorn, P. Buday, M. Heiland, A. Pannwitz, F. H. Schacher, W. Weigand, C. Streb and D. Ziegenbalg, *ChemPhotoChem*, 2022, **6**, e20220004.
- 22 T. D. Svejstrup, A. Chatterjee, D. Schekin, T. Wagner, J. Zach, M. J. Johansson, G. Bergonzini and B. K   nig, *ChemPhotoChem*, 2021, **5**, 808–814.
- 23 N. Qi, M. K. Wismer, D. V. Conway, S. W. Krska, S. D. Dreher and S. Lin, *React. Chem. Eng.*, 2022, **7**, 354–360.
- 24 H. E. Bonfield, K. Mercer, A. Diaz-Rodriguez, G. C. Cook, B. S. J. McKay, P. Slade, G. M. Taylor, W. X. Ooi, J. D. Williams, J. P. M. Roberts, J. A. Murphy, L. Schmermund, W. Kroutil, T. Mielke, J. Cartwright, G. Grogan and L. J. Edwards, *ChemPhotoChem*, 2020, **4**, 45–51.
- 25 N. B. Bissonnette, K. A. Ryu, T. Reyes-Robles, S. Wilhelm, J. H. Tomlinson, K. A. Crotty, E. C. Hett, L. R. Roberts, D. J. Hazuda, M. Jared Willis, R. C. Oslund and O. O. Fadeyi, *ChemBioChem*, 2020, **21**, 3555–3562.
- 26 N. Corrigan, L. Zhernakov, M. H. Hashim, J. Xu and C. Boyer, *React. Chem. Eng.*, 2019, **4**, 1216–1228.
- 27 P. P. Lampkin, B. J. Thompson and S. H. Gellman, *Org. Lett.*, 2021, **23**, 5277–5281.
- 28 F. Schiel, C. Peinsipp, S. Kornigg and D. B   se, *ChemPhotoChem*, 2021, **5**, 431–437.
- 29 J. R. Lamb, K. P. Qin and J. A. Johnson, *Polym. Chem.*, 2019, **10**, 1585–1590.
- 30 M. Gonz   lez-Esguevillas, D. F. Fern   ndez, J. A. Rinc   n, M. Barberis, O. de Frutos, C. Mateos, S. Garc   a-Cerrada, J. Agejas and D. W. C. Macmillan, *ACS Cent. Sci.*, 2021, **7**, 1126–1134.
- 31 K. N. Laponov, J. Lopes, M. Barlog, E. V. Astrova, A. V. Malkov and A. A. Lapkin, *Org. Process Res. Dev.*, 2014, **18**, 1443–1454.
- 32 M. Sezen-Edmonds, J. E. Tabora, B. M. Cohen, S. Zaretsky, E. M. Simmons, T. C. Sherwood and A. Ramirez, *Org. Process Res. Dev.*, 2020, **24**, 2128–2138.
- 33 G. D. Brown, D. Batalla, C. L. Cavallaro, H. L. Perez, S. T. Wroblewski and T. C. Sherwood, *React. Chem. Eng.*, 2022, **7**, 1945–1953.
- 34 T. Roeder, N. Frommknecht, A. H   ltzel and U. Tallarek, *React. Chem. Eng.*, 2022, **7**, 2035–2044.
- 35 A. E. Cassano, C. A. Martin, R. J. Brandi and O. M. Alfano, *Ind. Eng. Chem. Res.*, 1995, **34**, 2155–2201.
- 36 Python Software Foundation, Python, <https://www.python.org>, (accessed 31 December 2021).
- 37 S. K. Lam, A. Pitrou and S. Seibert, in *Proceedings of the Second Workshop on the LLVM Compiler Infrastructure in HPC – LLVM’15*, ACM Press, New York, USA, 2015, pp. 1–6.
- 38 C.-C. Sun, W.-T. Chien, I. Moreno, C.-T. Hsieh, M.-C. Lin, S.-L. Hsiao and X.-H. Lee, *Opt. Express*, 2010, **18**, 6137.
- 39 ThorLabs, Diffuser Kits, [https://www.thorlabs.com/NewGroupPage9\\_PF.cfm?Guide=10&Category\\_ID=220&ObjectGroup\\_ID=4780](https://www.thorlabs.com/NewGroupPage9_PF.cfm?Guide=10&Category_ID=220&ObjectGroup_ID=4780), (accessed 4 June 2022).
- 40 Photonics Media, Mirrors: Coating Choice Makes a Difference, [https://www.photonics.com/Articles/Mirrors\\_Coating\\_Choice\\_Makes\\_a\\_Difference/a25501](https://www.photonics.com/Articles/Mirrors_Coating_Choice_Makes_a_Difference/a25501), (accessed 4 June 2022).
- 41 S. Shanmugam, J. Xu and C. Boyer, *J. Am. Chem. Soc.*, 2015, **137**, 9174–9185.
- 42 J. Xu, K. Jung, A. Atme, S. Shanmugam and C. Boyer, *J. Am. Chem. Soc.*, 2014, **136**, 5508–5519.
- 43 B. Cortese, T. Noel, M. H. J. M. de Croon, S. Schulze, E. Klemm and V. Hessel, *Macromol. React. Eng.*, 2012, **6**, 507–515.
- 44 D. J. Walsh, D. A. Schinski, R. A. Schneider and D. Guironnet, *Nat. Commun.*, 2020, **11**, 3094.
- 45 N. Corrigan, A. Almasri, W. Taillades, J. Xu and C. Boyer, *Macromolecules*, 2017, **50**, 8438–8448.

